Article

Enhanced Photocatalytic Efficiency of N–F-Co-Embedded Titania under Visible Light Exposure for Removal of Indoor-Level Pollutants

Seung-Ho Shin [1], Ho-Hwan Chun [2] and Wan-Kuen Jo [1],*

[1] Department of Environmental Engineering, Kyungpook National University, Daegu 702-701, Korea; E-Mail: ssho@knu.ac.kr

[2] Department of Naval Architecture and Ocean Engineering, Pusan National University, 63 Jangjeon-dong, Geumjeong-gu, Busan 609-735, Korea; E-Mail: chunahh@pusan.ac.kr

* Author to whom correspondence should be addressed; E-Mail: wkjo@knu.ac.kr; Tel./Fax: +82-53-950-6584.

Abstract: N–F-co-embedded titania (N–F–TiO_2) photocatalysts with varying N:F ratios were synthesized and tested for their ability to photocatalyze the degradation of pollutants present at indoor air levels using visible light. The synthesis was achieved using a solvothermal process with tetrabutyl titanate, urea and ammonium fluoride as sources of Ti, N and F, respectively. Three selected volatile organic compounds (toluene, ethyl benzene and o-xylene) were selected as the test pollutants. The prepared composites were characterized using X-ray diffraction, energy-dispersive X-ray spectroscopy, X-ray photoelectron spectroscopy and Ultra-violet (UV)-visible spectroscopy. The photocatalytic degradation efficiencies of N–F–TiO_2 composites were higher than those obtained using pure TiO_2 and N–TiO_2. Moreover, these efficiencies increased as the N:F ratio decreased from sixteen to eight, then decreased as it dropped further to three, indicating the presence of an optimal N:F ratio. Meanwhile, as retention time decreased from 12.4 to 0.62 s, the average photocatalytic efficiencies decreased from 65.4% to 21.7%, 91.5% to 37.8% and 95.8% to 44.7% for toluene, ethyl benzene and o-xylene, respectively. In contrast, the photocatalytic reaction rates increased as retention time decreased. In consideration of all of these factors, under optimized operational conditions, the prepared N–F–TiO_2 composites could be utilized for the degradation of target pollutants at indoor air levels using visible light.

1. Introduction

Among semiconductors developed for photocatalytic applications, titanium dioxide (TiO_2) is most common because of its oxidizing potential, chemical inertness and high photo-resistance [1,2]. Nevertheless, practical applications for TiO_2 are limited by its wide band gap, which requires Ultra-violet (UV) radiation for photocatalytic activation [3]. As a result, much work has been directed at bringing the band gap energy difference to within the visible range throughout the use of metal [4,5] or non-metal [6–9] dopants. Certain metals, however, cause an increase in the number of recombination centers for photo-produced charge carriers, which results in thermal instability and a decrease in photocatalytic efficiency [10]. Furthermore, the toxic properties of heavy metals restrict later disposal.

Embedding TiO_2 with non-metal elements, including nitrogen (N), fluorine (F), carbon (C) and sulfur (S), is therefore a promising alternative approach [6–9]. N doping especially has been extensively investigated, chiefly owing to the fact that the atomic size of N is comparable to that of oxygen (O), in addition to it forming metastable centers, exhibiting low ionization energy and having high thermal stability [2,10,11]. While the exact mechanism for the activation of N-doped TiO_2 (N–TiO_2) is uncertain, it is generally ascribed to the narrowed band gap resulting from the integration of N 2p states that are higher in energy than the top of the valence band [12,13]. Additionally, N doping alters the surface structure of TiO_2 and controls the surface transfer of charge carriers, thereby enhancing photocatalytic performance [12,14]. Consequently, N–TiO_2 possesses superior photocatalytic activity under visible light irradiation when compared to pure TiO_2, allowing for the improved degradation of various pollutants, including aqueous rhodamine B, gaseous acetaldehyde and aromatic hydrocarbons [9,12,15,16].

In addition to N, F can increase the surface acidity of TiO_2, thereby improving photocatalytic performance [17]. Certain studies reported that F doping alone does not significantly shift the light absorption into the visible spectral range [13], while other studies found that single modified titania with F could induce enhanced visible light-driven photocatalytic activity for the degradation of gas-phase acetone or acid orange 7 [18,19]. This difference is ascribed to different experimental conditions, such as the synthesis method, the F-to-TiO_2 ratio, the target compound and the media. Regardless of this issue, in order to further take advantage of the benefits of N-doping, N–F-codoping of TiO_2 (N–F–TiO_2) has been developed [13,18–20]. When compared to single element doping, codoping strategies like this one that employed two elements, such as C and N [21] or Pt and N [22], have yielded higher photocatalytic activity.

Several studies have explored N–F–TiO_2 synthesis, relying on sol–gel [18–20], solvothermal [13] and single-step combustion [23] methods, employing many different conditions by varying the calcination temperature and the ratio of the heteroatoms to Ti. However, the effect of the F to N ratio remains unaddressed. Additionally, previous studies have focused only on the photocatalytic efficiency of the degradation of specific aqueous pollutants; the reaction mechanisms for these degradations may

be different outside of solution [24]. This study, therefore, addresses both of these issues, relying on a solvothermal route and analyzing the degradation of volatile organic compounds (VOCs) present at indoor levels under visible light irradiation. Pure TiO_2 and $N-TiO_2$ were also investigated for comparison. Toluene, ethyl benzene and o-xylene were chosen as the aromatic pollutants to be analyzed, because of their relatively high frequency in the selected environments [25] and the health hazards that they pose [26].

2. Results and Discussion

2.1. Characteristics of Prepared Photocatalysts

The $N-F-TiO_2$ composites employing varying N:F ratios, along with the pure TiO_2 and $N-TiO_2$ reference catalysts, were characterized by X-ray diffraction (XRD), energy dispersive X-ray analysis (EDX), X-ray photoelectron spectroscopy (XPS) and UV-visible spectroscopy (UV-Vis). The corresponding XRD patterns are shown in Figure 1. The $N-F-TiO_2$ composites, as well as the two reference photocatalysts, exhibited only anatase phase peaks at $2\theta = 25.3°, 37.9°, 47.9°, 53.9°, 62.7°$ and $70.3°$, consistent with previous studies [13,18], for samples calcined at or below 600 °C. Notably, both the $N-F-TiO_2$ and $N-TiO_2$ composites displayed a shift in the (101) crystal plane ($2\theta = 25.2°$), suggesting the presence of lattice distortion [18]. Based on the anatase (101) diffraction data, the crystalline sizes of pure TiO_2, $N-TiO_2$ and $N-F-TiO_2$ composites with N:F ratios of 16, 6, 6, 4 and 3 (referred to as $N-F-TiO_2$-16, $N-F-TiO_2$-8, $N-F-TiO_2$-6, $N-F-TiO_2$-4 and $N-F-TiO_2$-3, respectively) were estimated to be 14.1, 12.6, 13.2, 13.4, 13.7, 13.8 and 14.0 nm, respectively. The smaller crystal sizes for the doped samples are in line with the proposal that doping might somewhat suppress TiO_2 crystal growth [13].
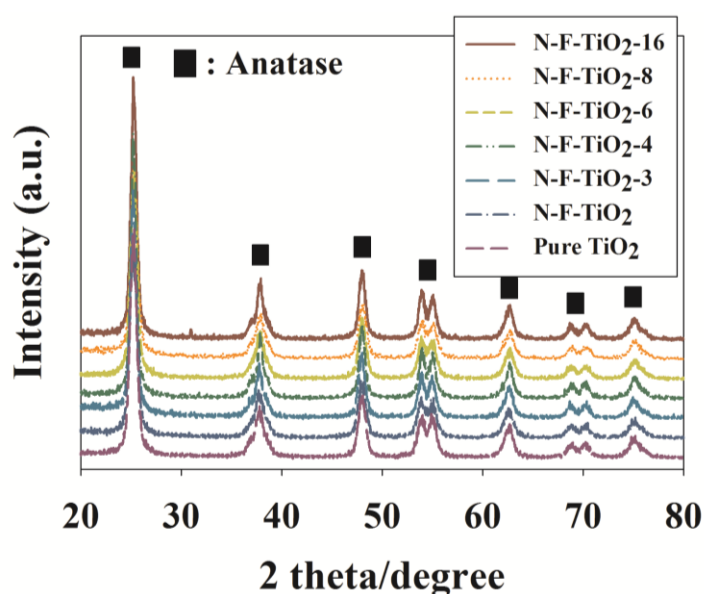
Figure 1. X-ray diffraction patterns of $N-F-TiO_2$ with different N:F ratios ($N-F-TiO_2$-3, $N-F-TiO_2$-4, $N-F-TiO_2$-6, $N-F-TiO_2$-8 and $N-F-TiO_2$-16), $N-TiO_2$ and pure TiO_2.

The chemical compositions of the photocatalyst samples were investigated with the help of XPS analyses. The XPS spectra confirmed the presence of both N and F in the N–F–TiO$_2$ composites (Figure 2). Table 1 shows the derived binding energies and the N and F concentrations for all tested samples. F1s peaks appeared at 684.1, 683.1, 683.9, 683.1 and 683.9 eV in N–F–TiO$_2$-16, N–F–TiO$_2$-8, N–F–TiO$_2$-6, N–F–TiO$_2$-4 and N–F–TiO$_2$-3, respectively; these peaks likely result from F$^-$ ions adsorbed onto the TiO$_2$ surface [20]. In addition, the F1s peak at 688 eV was assigned to F atoms that substituted for O sites within the TiO$_2$ lattice (data not shown) [13]. Meanwhile, the N1s peaks were observed at 399.4, 399.2, 399.4, 399.4 and 399.4 eV for N–F–TiO$_2$-16, N–F–TiO$_2$-8, N–F–TiO$_2$-6, N–F–TiO$_2$-4 and N–F–TiO$_2$-3, respectively; these were associated with molecularly chemisorbed N atoms [12]. The XPS data also revealed Ti2s, Ti2p, Ti3s, Ti3p and O1s peaks at 565.5–567.2, 459.1–459.9, 61.5–62.9, 37.7, and 529.2–529.8 eV, respectively. Pelaez *et al.* [20] have reported, based on XPS results, that N and F atoms can be successfully embedded into TiO$_2$ using a fluorosurfactant-based sol-gel process.
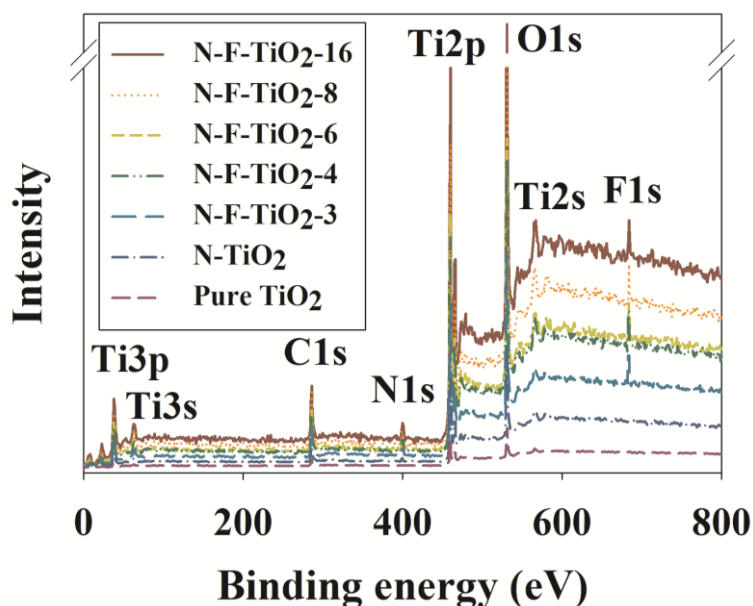
Figure 2. X-ray photoelectron spectroscopy of N–F–TiO$_2$ with different N:F ratios (N–F–TiO$_2$-3, N–F–TiO$_2$-4, N–F–TiO$_2$-6, N–F–TiO$_2$-8 and N–F–TiO$_2$-16), N–TiO$_2$ and pure TiO$_2$.

Table 1. Binding energy (eV) and amounts (%) of N and F for N–F–TiO$_2$-3, N–F–TiO$_2$-4, N–F–TiO$_2$-6, N–F–TiO$_2$-8, N–F–TiO$_2$-16, N–TiO$_2$ and pure TiO$_2$ *.

Photocatalyst	Ti2p	Ti3p	Ti2s	Ti3s	O1s	N1s	F1s
N–F–TiO$_2$-16	459.9	37.7	566.1	62.6	529.8	399.4 (7.2)	684.1 (0.4)
N–F–TiO$_2$-8	459.9	37.7	567.2	62.6	529.4	399.2 (6.9)	683.1 (0.8)
N–F–TiO$_2$-6	459.9	37.7	565.5	61.5	529.2	399.4 (7.0)	683.9 (1.3)
N–F–TiO$_2$-4	459.7	37.7	566.2	62.6	529.2	399.4 (7.4)	683.1 (1.7)
N–F–TiO$_2$-3	459.1	37.7	566.1	62.9	529.4	399.4 (6.8)	683.9 (2.1)
N–TiO$_2$	459.1	37.7	567.1	62.6	529.8	NA	NA
pure TiO$_2$	459.7	37.7	566.1	62.8	529.8	NA	NA

* Numbers in parenthesis represent the amounts (%) of N or F; NA, not available.

Figure 3 displays the UV-Vis absorption spectra of the tested samples. Pure TiO_2 showed an absorption edge at approximately 410 nm, a value that is in agreement with previous studies [15,27]. In contrast, the absorption spectra of both the $N–TiO_2$ and $N–F–TiO_2$ composites shifted toward the visible region, with values of 449.2, 456.4, 461.5, 471.1, 477.5 and 483.9 nm for $N–TiO_2$, $N–F–TiO_2$-3, $N–F–TiO_2$-4, $N–F–TiO_2$-6, $N–F–TiO_2$-8 and $N–F–TiO_2$-16, respectively. This effect was attributed to the impurity states at the substitutional lattice sites resulting from N integration [12,13,28]. Additionally, visible light absorption intensity was greater for $N–F–TiO_2$ than for $N–TiO_2$, while also increasing gradually as the N:F ratios decreased. Di Valentin *et al*. [19] also reported that the visible light absorption increased gradually as the N:F ratios decreased from to 100 to 1.0 in $N–F–TiO_2$ composites, which were prepared by a sol–gel process. Both of these effects were attributed to some kind of synergistic effect, given that F alone usually does not derive efficient light absorption.
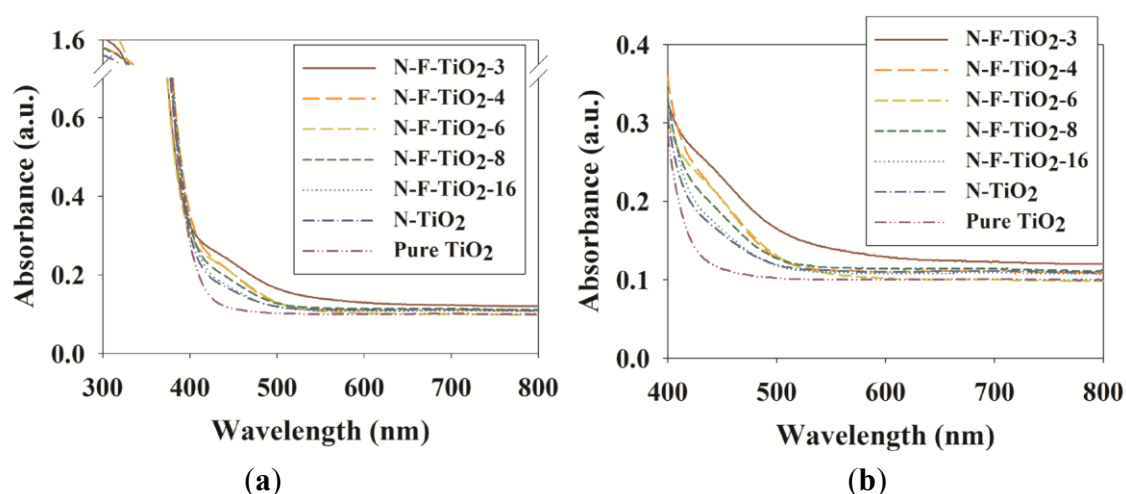
Figure 3. (**a**) UV-Vis spectra of $N–F–TiO_2$ with different N:F ratios ($N–F–TiO_2$-3, $N–F–TiO_2$-4, $N–F–TiO_2$-6, $N–F–TiO_2$-8 and $N–F–TiO_2$-16), $N–TiO_2$ and pure TiO_2; (**b**) The enlarged scale of the spectra is also provided.

2.2. Photocatalytic Activities of N–F–TiO2, N–TiO2 and Pure TiO2

The photocatalytic activities of the fabricated materials were investigated by exposure to visible light after allowing for adsorption in the dark. A control test performed using an uncoated Pyrex tube under visible light irradiation showed insignificant photolysis of the target compounds. Figure 4 shows time series of the photocatalytic degradation efficiencies (PDEs) of toluene, ethyl benzene and o-xylene for both reference photocatalysts and the assorted $N–F–TiO_2$ composites under visible light exposure. $N–F–TiO_2$ showed the highest activity, with average PDEs of 29.1%, 49.6% and 60.2% for toluene, ethyl benzene and o-xylene, respectively. $N–TiO_2$ showed decreased activity of 17.4%, 25.3% and 34.2%, respectively, while pure TiO_2 was the least active, with values of 15.7%, 18.7% and 20.4%, respectively. Previous studies have compared $N–F–TiO_2$ performance with that of Degussa P25 TiO_2, prepared TiO_2, $N–TiO_2$ and $F–TiO_2$ and have demonstrated improved activity for the degradation of acetic orange, methyl orange methylene blue and microcystin in aqueous media [13,18–20,23]; again, this enhanced activity was ascribed to synergistic effects.
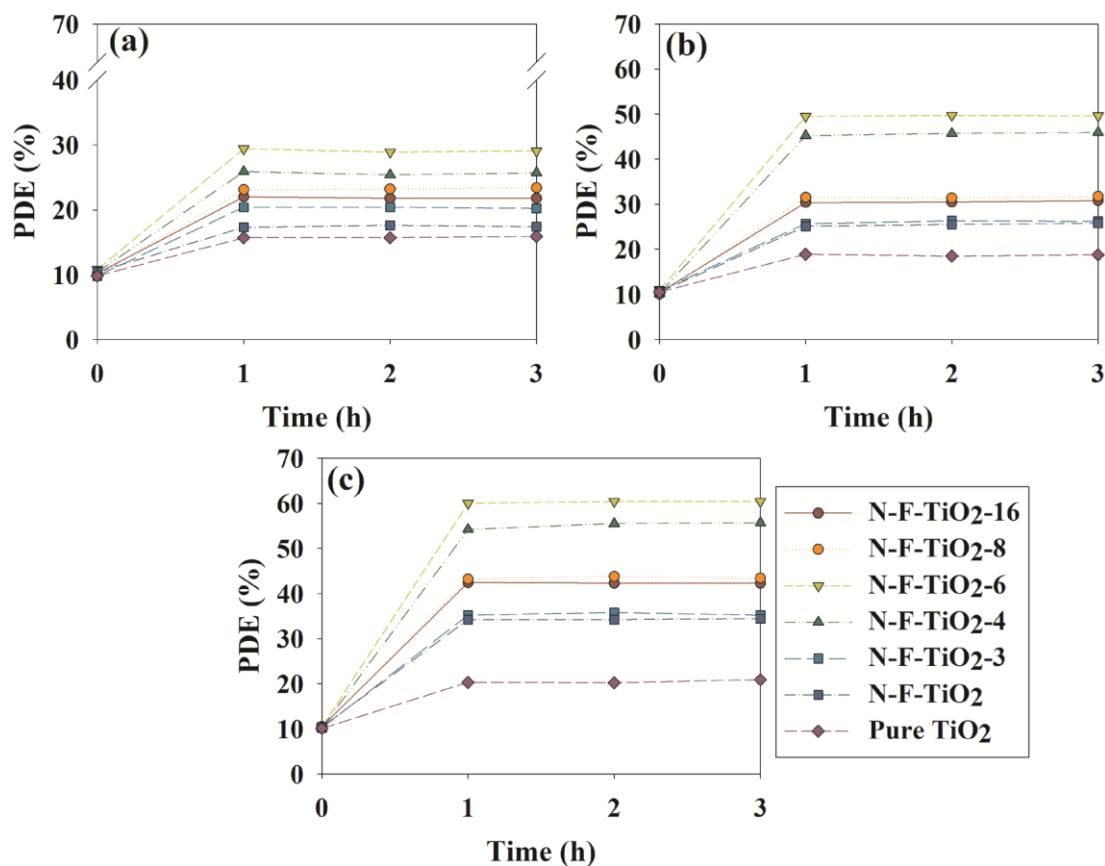
Figure 4. Time-series photocatalytic degradation efficiencies (PDEs, %) of (**a**) toluene, (**b**) ethyl benzene and (**c**) o-xylene as determined using N–F–TiO$_2$ with different N:F ratios (N–F–TiO$_2$-3, N–F–TiO$_2$-4, N–F–TiO$_2$-6, N–F–TiO$_2$-8 and N–F–TiO$_2$-16), N–TiO$_2$ and pure TiO$_2$.

Figure 4 also outlines the performance dependence on N:F ratios, with PDEs increasing as the N:F ratio decreased from sixteen to six. This pattern again suggests increasing synergy with increasing F content. However, the value then proceeded to drop as the N:F ratio decreased from six to three; this effect has been previously attributed to excess F species acting as an inhibitor by screening the TiO$_2$ surface or capturing photon-generated holes [20]. Notably, N–F–TiO$_2$-6 exhibited the highest PDEs, even though it absorbed less light than N–F–TiO$_2$-4 and N–F–TiO$_2$-3, suggesting that the photocatalytic activity is not strictly dependent on visible light absorption.

Figure 5 shows time series of the PDEs for toluene, ethyl benzene and o-xylene obtained for N–F–TiO$_2$-6 under visible light exposure based on retention time, demonstrating a positive correlation. Specifically, the average PDEs for toluene decreased from 65.4% to 21.7% as the retention time decreased from 12.40 to 0.62 s. This agrees with previous research by Jo and Kang [29], who reported that the PDEs of select aromatic vapors treated with polyacrylonitrile-supported TiO$_2$ fibers decreased gradually with retention time. Retention times were estimated by dividing the reactor volume by the air flow rate. The low PDEs for low retention time conditions were ascribed to short reaction times inside the continuous-flow Pyrex reactor.
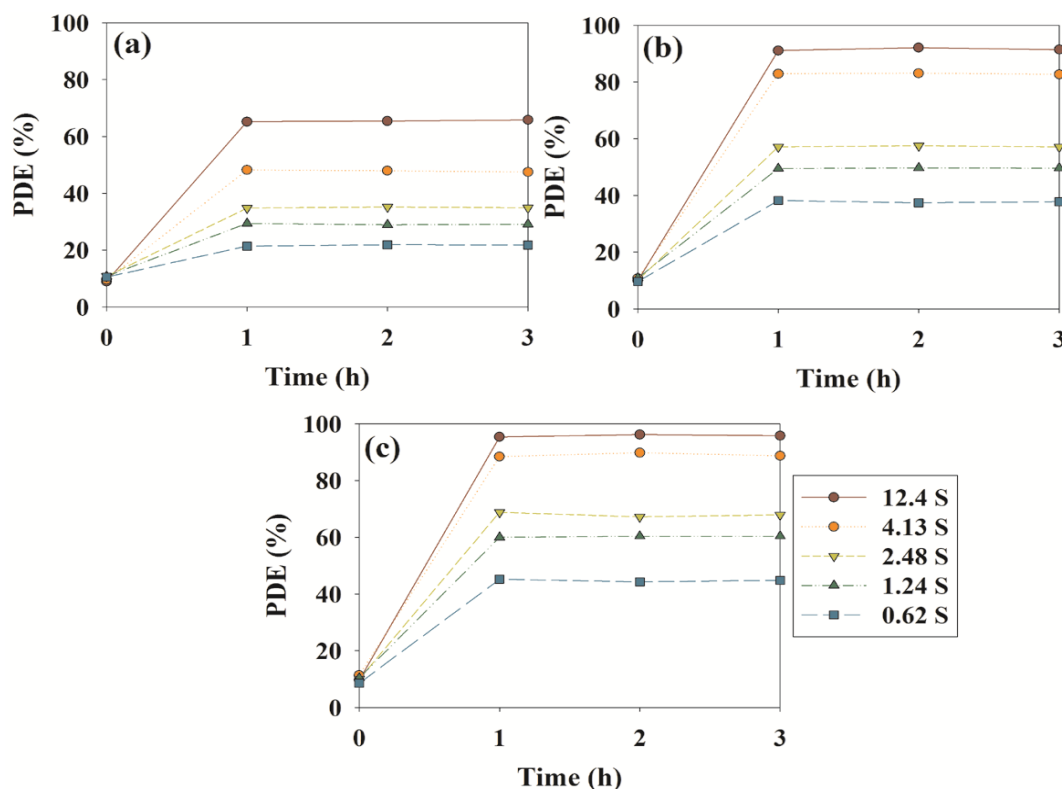
Figure 5. Time-series photocatalytic degradation efficiencies (PDEs, %) of (**a**) toluene, (**b**) ethyl benzene and (**c**) o-xylene as determined using N–F–TiO$_2$-6, according to retention time.

The photocatalytic reaction rates were estimated by combining the retention times with the following equation:

$$r_R = f_c \cdot (C_i - C_o) Q_{air}/A_c \tag{1}$$

where r_R represents the photocatalytic reaction rate (PRR) (μmol·m^{-2}·s^{-1}), C_i and C_o represent the upstream and downstream concentrations of each target chemical (ppm), respectively, Q_{air} represents the airstream flow rate (m^3·s^{-1}), A_c represents the inner-wall area coated with the photocatalyst (m^2) and f_c represents the conversion coefficient (40.9 μmol·m^{-3}·ppm^{-1}). Unlike the PDEs, the PRRs increased as retention time decreased (Table 2), with values for toluene of 0.2×10^{-3} and 1.0×10^{-3} for retention times of 12.4 and 0.62 s, respectively. Previous studies reported the same pattern, suggesting that PRRs are affected by the mass transfer effect, a phenomenon that is closely associated with heterogeneous reaction kinetics [29,30]. Consequently, the dependence of PRRs on retention time was not assigned to photocatalyst surface reactions.

Table 2. Reaction rates (μmol·m^{-2}·s^{-1}) of three target compounds obtained using the N–F–TiO$_2$-6 according to retention time.

Compound	Retention Time (s)				
	0.62	**1.24**	**2.48**	**4.13**	**12.4**
Toluene	1.0×10^{-3}	0.7×10^{-3}	0.4×10^{-3}	0.3×10^{-3}	0.2×10^{-3}
Ethyl benzene	1.8×10^{-3}	1.2×10^{-3}	0.7×10^{-3}	0.5×10^{-3}	0.2×10^{-3}
o-Xylene	2.1×10^{-3}	1.4×10^{-3}	0.8×10^{-3}	0.5×10^{-3}	0.2×10^{-3}

3. Experimental Section

3.1. Synthesis and Characterization of Photocatalysts

N–F–TiO$_2$ photocatalysts with varying N:F ratios were synthesized by a solvothermal method, using tetrabutyl titanate (TBT, Ti(OC$_4$H$_9$)$_4$), urea (CO(NH$_2$)$_2$) and ammonium fluoride (NH$_4$F) as sources of Ti, N and F, respectively. TBT (9 mL, 97%, Sigma-Aldrich, St. Louis, MO, USA) was added to ethyl alcohol (32 mL, 99.9%, Sigma-Aldrich) and concentrated nitric acid (0.4 mL, 69%, Merck, Whitehouse Station, NJ, USA). In addition, urea (0.22 g, 99%, Sigma-Aldrich), ammonium fluoride (98%, Sigma-Aldrich) and deionized water (2 mL) were added to ethyl alcohol (70 mL). The synthesis of N–F–TiO$_2$-16, N–F–TiO$_2$-8, N–F–TiO$_2$-6, N–F–TiO$_2$-4 and N–F–TiO$_2$-3 required the use of 0.014, 0.028, 0.042, 0.056 and 0.084 g, respectively, of ammonium fluoride. Subsequently, the former solution was slowly added to the latter under magnetic stirring. After further stirring of the mixture at room temperature for 2 h, it was hydrothermally treated in an autoclave (150 mL) at 150 °C for 20 h. Finally, the treated mixture was washed with deionized water, dried at 100 °C overnight and treated at 400 °C for 3 h to obtain the desired N–F–TiO$_2$ powder. Pure TiO$_2$ and N–TiO$_2$ were prepared following the same procedure, but without the addition of the corresponding element sources. It is worth noting that the so-called N:F ratio was only the ratio of precursors, which were highly unlikely to be the same as the composition of the resulting photocatalysts. The prepared photocatalysts were examined by XRD (Rigaku D/max-2500 diffractometer, Tokyo, Japan), XPS (PHI Quantera SXM, Chanhassen, MN, USA) and UV-Vis (Varian CARY 5G, Santa Clara, CA, USA).

3.2. Tests for Photocatalytic Activity

The photocatalytic activities of the synthesized photocatalysts were tested using a plug-flow Pyrex reactor (3.8 cm i.d. and 26.0 cm length) with an inner wall coated in a thin film of the appropriate catalyst. To apply the coatings, titanium tetra-isopropoxide (50 mL, 97%, Sigma-Aldrich) was first added to glacial acetic acid (10 mL, 99%, Sigma-Aldrich) under stirring. The resulting solution was mixed with 1000 mL deionized water and then 10 mL nitric acid (98%, Sigma-Aldrich), stirred until a white precipitate was obtained and then heated at 80 °C for 5 h in a bath to obtain a sol. The selected, previously synthesized photocatalyst (2 g) was then added to the sol, after which the mixture was sonicated for 30 min to afford a sol coating. The outer wall of the Pyrex reactor was wrapped with a commercially-available vinyl sheet and dipped in the coating for 10 min, after which it was removed at a rate of 2 cm min^{-1} and kept in a clean room for 3 h. The coating and drying process was performed three times to maximize coating. A cylindrical lamp (F8T5DL, Youngwha Lamp Co., Seoul, Korea) designed to simulate daylight was placed in the coated reactor. A pure dried air stream provided from a compressed air tank was humidified by passing it through impingers, while the desired 0.1 ppm standard gas concentration was achieved by mixing the humidified air with the target chemicals, which were injected into a glass chamber via a syringe pump (Model Legato 100, KdScientific, Holliston, MA, USA). The prepared gas was routed into an empty buffering bulb (1 L) to minimize fluctuations in the supplied gas concentrations, after which it was fed into the reactor.

The photocatalytic decomposition efficiencies of the prepared photocatalysts were examined under a fixed stream flow rate of 1 L min^{-1} and a relative humidity of 45%, representative of a comfortable

humidity level. The intensity of supplied light was 0.5 mW cm^{-2} at a distance from the lamp to the inner wall of the reactor. In addition, the PDE of N–F–TiO$_2$-6, which was selected as representative of the N–F–TiO$_2$ photocatalysts, because it showed the highest activity, was examined under retention times of 0.62, 1.24, 2.48, 4.13 and 12.4 s. All other parameters were adjusted to the values described above. Each experiment was conducted in triplicate.

Gas concentration measurements were completed upstream and downstream from the reactor. Samples were collected by drawing air from sampling ports fitted with Tenax adsorbent traps. Gases that had been adsorbed on the Tenax were pretreated using a thermal desorbing system (Perkin Elmer ATD 350, Llantrisant, UK) and analyzed by a gas chromatograph/mass spectrometer (Perkin Elmer Clarus SQ 8) outfit with a capillary column (DB-5, Agilent, Santa Clara, CA, USA). The target compounds were qualitatively determined on the basis of their retention times and mass spectra (Wiley 275 software library). Quantification of gaseous compounds was carried out using calibration curves, which were established using four concentrations normalized to an internal standard. Laboratory blanks and spiked adsorbent traps were used for the quality control of these analyses, with one blank trap analyzed on the day of the experimentation to check for any contamination. The detection limits of the target pollutants ranged from 0.002 to 0.005 ppm, depending on the chemical.

4. Conclusions

In this study, N–F–TiO$_2$ photocatalysts with varying N:F ratios were synthesized and analyzed for their visible range photocatalytic performance in the degradation of VOCs present at standard indoor air concentrations. XPS demonstrated the successful integration of N and F into the TiO$_2$, while UV-Vis spectra of both the N–F–TiO$_2$ samples and the N–TiO$_2$ control demonstrated improved visible light absorption. The N–F–TiO$_2$ composites displayed superior photocatalytic degradation of toluene, ethyl benzene and o-xylene when compared to pure and N–TiO$_2$, with precise activity dependent on the N:F ratio. In addition, retention time was found to be a significant factor affecting performance. Overall, these results indicate the utility of the prepared N–F–TiO$_2$ composites under optimized operational conditions.

Acknowledgments

Author Contributions

Wan-Kuen Jo established the research protocol and analyzed the experimental data. Seung-Ho Shin performed experimental works, and Ho-Hwan Chun assisted in data analysis.

Conflicts of Interest

The authors declare no conflict of interest.

References

1. Nakata, K.; Fujishima, A. TiO₂ photocatalysis: Design and applications. *J. Photochem. Photobiol. C* **2012**, *13*, 169–189.
2. Devi, L.G.; Kavitha, R. A review on non metal ion doped titania for the photocatalytic degradation of organic pollutants under UV/solar light: Role of photogenerated charge carrier dynamics in enhancing the activity. *Appl. Catal. B* **2013**, *140–141*, 559–587.
3. Henderson, M.A. A surface science perspective on TiO₂ photocatalysis. *Surf. Sci. Rep.* **2011**, *66*, 185–297.
4. Guo, H.; Kemell, M.; Heikkilä, M.; Leskelä, M. Noble metal-modified TiO₂ thin film photocatalyst on porous steel fiber support. *Appl. Catal. B* **2010**, *95*, 358–364.
5. Kment, S.; Kmentova, H.; Kluson, P.; Krysa, J.; Hubicka, Z.; Cirkva, V.; Gregora, I.; Solcova, O.; Jastrabik, L. Notes on the photo-induced characteristics of transition metal-doped and undoped titanium dioxide thin films. *J. Colloid Interface Sci.* **2010**, *348*, 198–205.
6. Ohno, T.; Akiyoshi, M.; Umebayashi, T.; Asai, K.; Mitsui, T.; Matsumura, M. Preparation of S-doped TiO₂ photocatalysts and their photocatalytic activities under visible light. *Appl. Catal. A* **2004**, *265*, 115–121.
7. Sun, H.; Wang, S.; Ang, H.M.; Tadé, M.O.; Li, Q. Halogen element modified titanium dioxide for visible light photocatalysts. *Chem. Eng. J.* **2010**, *162*, 437–447.
8. Matos, J.; García, A.; Zhao, L.; Titirici, M.M. Solvothermal carbon-doped TiO₂ photocatalyst for the enhanced methylene blue degradation under visible light. *Appl. Catal. A* **2010**, *390*, 175–182.
9. Hu, C.-C.; Hsu, T.-C.; Lu, S.-Y. Effect of nitrogen doping on the microstructure and visible light photocatalysis of titanate nanotubes by a facile cohydrothermal synthesis via urea treatment. *Appl. Surf. Sci.* **2013**, *280*, 171–178.
10. Di Valentin, C.; Finazzi, E.; Pacchioni, G.; Selloni, A.; Livraghi, S.; Paganini, M.C.; Giamello, E. N-doped TiO₂: Theory and experiment. *Chem. Phys.* **2007**, *338*, 44–56.
11. Pelaez, M.; Nolan, N.T.; Pillai, S.C.; Seery, M.K.; Falaras, P.; Kontos, A.G.; Dunlop, P.S.M.; Hamilton, J.W.J.; Byrne, J.A.; O'Shea, K.; *et al.* A review on the visible light active titanium dioxide photocatalysts for environmental applications. *Appl. Catal. B* **2012**, *125*, 331–349.
12. Asahi, R.; Morikawa, T.; Ohwaki, T.; Aoki, K.; Taga, Y. Visible-light photocatalysis in nitrogen-doped titanium oxides. *Science* **2001**, *293*, 269–271.
13. Wu, Y.; Xing, M.; Tian, B.; Zhang, J.; Chen, F. Preparation of nitrogen and fluorine co-doped mesoporous TiO₂ microsphere and photodegradation of acid orange 7 under visible light. *Chem. Eng. J.* **2010**, *162*, 710–717.
14. Liu, G.; Wang, X.; Wang, L.; Chen, Z.; Li, F.; Lu, G.Q.; Cheng, H.-M. Drastically enhanced photocatalytic activity in nitrogen doped mesoporous TiO₂ with abundant surface states. *J. Colloid Interface Sci.* **2009**, *334*, 171–175.
15. Jo, W.K.; Kim, J.T. Application of visible-light photocatalysis with nitrogen-doped or unmodified titanium dioxide for control of indoor-level volatile organic compounds. *J. Hazard. Mater.* **2009**, *164*, 360–366.

16. Gurkan, Y.Y.; Turkten, N.; Hatipoglu, A.; Cinar, Z. Photocatalytic degradation of cefazolin over N-doped TiO_2 under UV and sunlight irradiation: Prediction of the reaction paths via conceptual DFT. *Chem. Eng. J.* **2012**, *184*, 113–124.

17. Tang, J.; Quan, H.; Ye, J. Photocatalytic properties and photoinduced hydrophilicity of surface-Fluorinated TiO_2. *Chem. Mater.* **2007**, *19*, 116–122.

18. Sun, H.; Zhou, G.; Liu, S.; Ang, H.M.; Tadé, M.O.; Wang, S. Visible light responsive titania photocatalysts codoped by nitrogen and metal (Fe, Ni, Ag, or Pt) for remediation of aqueous pollutants. *Chem. Eng. J.* **2013**, *231*, 18–25.

19. Di Valentin, C.; Finazzi, E.; Pacchioni, G. Density functional theory and electron paramagnetic resonance study on the effect of N–F codoping of TiO_2. *Chem. Mater.* **2008**, *20*, 3706–3714.

20. Pelaez, M.; de la Cruz, A.A.; Stathatos, E.; Falaras, P.; Dionysiou, D.D. Visible light-activated N–F-codoped TiO_2 nanoparticles for the photocatalytic degradation of microcystin-LR in water. *Catal. Today* **2009**, *144*, 19–25.

21. Cong, Y.; Chen, F.; Zhang, J.L.; Anpo, M. Carbon and nitrogen-codoped TiO_2 with high visible light photocatalytic activity. *Chem. Lett.* **2006**, *35*, 800–801.

22. Sun, H.; Ullah, R.; Chong, S.; Ang, H.M.; Tadé, M.O.; Wang, S. Room-light-induced indoor air purification using an efficient $Pt/N-TiO_2$ photocatalyst. *Appl. Catal. B* **2011**, *108–109*, 127–133.

23. Wu, G.; Wen, J.; Nigro, S.; Chen, A. One-step synthesis of N- and F-codoped mesoporous TiO_2 photocatalysts with high visible light activity. *Nanotechnology* **2010**, *21*, doi:10.1088/0957-4484/21/8/085701.

24. Fujishima, A.; Zhang, X.; Tryk, D.A. TiO_2 photocatalysis and related surface phenomena. *Surf. Sci. Rep.* **2008**, *63*, 515–582.

25. Schlink, U.; Thiem, A.; Kohajda, T.; Richter, M.; Strebel, K. Quantile regression of indoor air concentrations of volatile organic compounds (VOC). *Sci. Total Environ.* **2010**, *408*, 3840–3851.

26. USEPA. An Introduction to Indoor Air Quality: Volatile Organic Compounds (VOCs). Available online: http://www.epa.gov/iaq/voc.html (accessed on 11 December 2012).

27. Sun, S.; Ding, J.; Bao, J.; Gao, C.; Qi, Z.; Yang, X.; He, B.; Li, C. Photocatalytic degradation of gaseous toluene on $Fe–TiO_2$ under visible light irradiation: A study on the structure, activity and deactivation mechanism. *Appl. Surf. Sci.* **2012**, *258*, 5031–5037.

28. Li, D.; Haneda, H.; Hishita, S.; Ohashi, N. Visible-light-deriven NF-codoped TiO_2 photocatalysts. 2. Optical characterization, photocatalysis, and potential application to air purification. *Chem. Mater.* **2005**, *17*, 2596–2602.

29. Jo, W.K.; Kang, H.J. Polyacrylonitrile-TiO_2 fibers for control of gaseous aromatic compounds. *Ind. Eng. Chem. Res.* **2013**, *52*, 4475–4483.

30. Yu, K.-P.; Lee, G.W.M.; Huang, W.-M.; Wu, C.; Yang, S. The correlation between photocatalytic performance and chemical/physical properties of indoor volatile organic compounds. *Atmos. Environ.* **2006**, *40*, 375–385.